

Model-Based Analysis of the Influence of Forest Structures on the Scattering Phase Center at L-Band

Wenjian Ni, *Member, IEEE*, Guoqing Sun, *Senior Member, IEEE*, Kenneth Jon Ranson, Zhiyu Zhang, Yating He, Wenli Huang, and Zhifeng Guo

Abstract—The estimation of forest biomass from synthetic aperture radar (SAR) data is limited by the lack of forest structure information. Interferometric synthetic aperture radar (InSAR) provides a means for the extraction of forest structure. The crucial issue in InSAR application is to parameterize forest structure and to link the parameter with InSAR observations. Model-based analysis enables exploring the theoretical linkages between InSAR observations and forest structure free from temporal decorrelation effects. In this paper, a semicoherent model (SCSR) was first developed and verified. A series of simulations at L-band was then made for both homogeneous and heterogeneous forests generated from a forest growth model. The forest structure was parameterized by four height indices. Aside from the height of scattering phase center (HSPC), the depth of scattering phase center (DSPC) was also proposed to characterize the scattering phase center of InSAR. The results showed that the behavior of homogeneous forest on InSAR data was quite different from that of heterogeneous forest. Special care was needed when the retrieval algorithms of forest biomass developed on a homogeneous forest were applied to a heterogeneous forest. Crown size-weighted height (CWH) and Lorey's height were correlated with the HSPC at all polarizations and with the DSPC at copolarization in both cases of homogeneous and heterogeneous forests. These findings indicated that CWH could be an alternative biomass indicator of the Lorey's height for biomass estimation, which can be derived from the combination of InSAR data and the elevation of the forest canopy top from lidar or high-resolution stereo images.

Manuscript received July 8, 2012; revised June 11, 2013; accepted July 24, 2013. This work was supported in part by the National Basic Research Program of China under Grant 2013CB733404, by the National Natural Science Foundation of China under Grants 41001208, 40971203, 41171283, and 91125003, by the National High-Tech R&D Program of China under Grant 2012AA12A306, by the Strategic Priority Research Program—Climate Change: Carbon Budget and Related Issues of the Chinese Academy of Sciences under Grant XDA05050100, and by the Terrestrial Ecology Program under Grant NNX09AG66G.

W. Ni was with the State Key Laboratory of Remote Sensing Science, jointly sponsored by the Institute of Remote Sensing and Digital Earth, Chinese Academy of Sciences, and Beijing Normal University, Beijing 100101, China. He is now with the Department of Geographical Sciences, University of Maryland, College Park, MD 20742 USA.

G. Sun and W. Huang are with the Department of Geographical Sciences, University of Maryland, College Park, MD 20740 USA.

K. J. Ranson is with the NASA Goddard Space Flight Center, Greenbelt, MD 20771 USA.

Z. Zhang and Z. Guo are with the State Key Laboratory of Remote Sensing Science, jointly sponsored by the Institute of Remote Sensing and Digital Earth, Chinese Academy of Sciences, and Beijing Normal University, Beijing 100101, China (e-mail: zhangzy@irsa.ac.cn).

Y. He is with the Institute of Agricultural Resources and Regional Planning, Chinese Academy of Agricultural Sciences, Beijing 100081, China.

Color versions of one or more of the figures in this paper are available online at <http://ieeexplore.ieee.org>.

Digital Object Identifier 10.1109/TGRS.2013.2278171

Index Terms—Canopy height, depth of scattering phase center (DSPC), forest structure, height of scattering phase center (HSPC), interferometric synthetic aperture radar (InSAR).

I. INTRODUCTION

THE exchange of carbon between forests and atmosphere is a vital component of the global carbon cycle. Accurate estimates of terrestrial carbon storage are required to determine its role in the global carbon cycle, to estimate the effect of anthropogenic disturbances (i.e., land use/land cover changes) on the cycle, and to monitor mitigation efforts that rely on carbon sequestration through reforestation [1]. The estimation of forest biomass from SAR data is limited by the lack of forest structure information. Interferometric synthetic aperture radar (InSAR) is a potential tool for the extraction of forest structure because it is sensitive to the vertical distribution of forest components over forested areas. The digital elevation model derived from InSAR is typically the elevation of the scattering phase center (SPC) rather than that of the bare ground surface. The SPC is located at a certain position between the forest canopy top and ground surface. It will change along with the SAR system parameters, understory conditions, and forest structures. There is consensus that the SPC of short-wavelength data (such as X- or C-band) should be located within the forest canopy while that of long-wavelength data should be lower due to its deeper penetration. Some researchers have successfully estimated the forest height using the dependence of the SPC on wavelength. Neeff *et al.* [2] used the difference between the digital terrain model from the X-band and the P-band InSAR data as a measure of vegetation height in the estimation of forest biomass. Balzter *et al.* [3] used the X-band and L-band InSAR data acquired by Experimental Synthetic Aperture Radar (E-SAR) airborne sensors to estimate the top heights of forest stands. Praks *et al.* [4] presented results from the Finnish Synthetic Aperture Radar (FinSAR) project, where the E-SAR (operating at the L- and X-bands) and the Helsinki University of Technology Scatterometer (operating at the X- and C-bands) instruments were operated together to validate tree-height retrieval algorithms for boreal forest. Aside from the dependence of the SPC on wavelength, its dependence on polarization [i.e., polarimetric SAR interferometry (PolInSAR)] is currently a hot topic in the retrieval of forest vertical structures. PolInSAR technology allows the separation of ground/forest phase centers through the selection of proper polarimetric basis and polarimetric combinations. Although PolInSAR is a new and advanced technology, it is still very important to explore algorithms for the estimation of forest biomass using single- or dual-polarization InSAR for heterogeneous forest because

there has been and will be near global coverage of such kind of data acquired, for example, by the Phased Array type L-band Synthetic Aperture Radar (PALSAR) onboard Advanced Land Observing Satellite (ALOS) (under fine mode single polarization or fine beam double polarization) and ALOS/PALSAR-2 (under fine beam dual polarization).

A crucial step for the exploration of such kind of algorithms is to find parameters which are a good description of the physical state of forest structures as well as correlated with InSAR observations. However, the mixture of contributions from upper and lower parts of forests complicates the interpretation of long-wavelength InSAR data. Model simulation is a powerful tool to provide an insight into the influencing mechanism of forest structure on the SPC. Meanwhile, model-based analysis may liberate the exploration of the theoretical linkage between InSAR observations and forest structures from the disturbance of temporal decorrelation that extensively existed in repeat-pass InSAR data. Several such kinds of models have been developed for the purpose. Thirion *et al.* proposed a forest coherent scattering model [5], which was based on a layered forest scene. The model was used to investigate the behavior of the interferometric phase center height along with frequency and the attenuation coefficients [6]. Liu *et al.* developed a 3-D coherent model based on realistic forest scenes [7]. The influence of forest type (i.e., conifer forest, broadleaf forest, and mixed forest) as well as the horizontal arrangement of trees (i.e., clump, regular, and random) on the position of the SPC were analyzed by the model simulations [8]. Garestier and Toan modified the random volume over ground (RVoG) model by vertically varying the extinction in the volume layer to integrate vertical heterogeneity in forest models [9]. It can be seen that, in these research works, the vertical heterogeneity is mainly defined by varied extinctions. Although the volume extinction is easy to be taken into account in models, it is not intuitive for the development of retrieval algorithms of forest height because the correlation between volume extinction and forest height is unknown and should be explored based on theoretical models. These research works are either based on a layered canopy model or realistic tree model. The layered model cannot fully describe the horizontal and vertical structures of forest. The realistic tree model requires more input information on a 3-D forest scene; for example, the size and position of each needle or leaf should be specified, so the computation load is heavy. The radar backscatter model by Sun and Ranson was built on a 3-D forest scene, which was constituted by cubic cells [10]. The interactions between leaves/needles and branches within a cubic cell were ignored while those between cubic cells were considered. It provides a balance between the layered and the realistic forest scene. If this 3-D model can be modified into a coherent or semicoherent backscattering model, the influence of forest structures on the SPC can be simulated with less computation loads.

In this paper, a semicoherent model was first developed based on the Sun and Ranson model [10] in Section II. The model was referred to as the semicoherent Sun and Ranson (SCSR) model. It was first verified by a layered forest scene at L-band and by the shuttle radar topography mission (SRTM) data at C-band in Section III. Section IV describes the model-based analysis of the influence of forest structures on the SPC followed by discussions and conclusions.

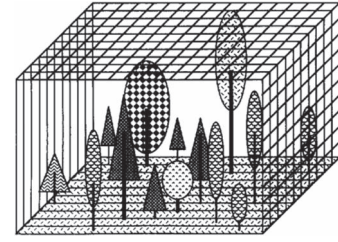


Fig. 1. Conceptual diagram of 3-D forest scene model.

II. MODEL DESCRIPTION

A. Description of Forest Scene

The forest scene characteristics used in the Sun and Ranson model will be kept in the SCSR model [10]. The inputs of the model include the position, size, species, and crown shape of each tree. The position and diameter at breast height (DBH) of trees can be obtained from field measurements or forest growth models. Regression relationships developed from field data are used to estimate the tree height, crown depth, and width from DBH. The dielectric constants can be specified for different species and for different environmental conditions. In the model, tree crown shapes are modeled as simple conical, ellipsoidal, and half-ellipsoidal shapes, depending on the tree species. The 3-D forest scene is constituted by the stack of cubic cells as shown in Fig. 1. The constituents of cubic cells are determined by their positions. The cubic cell located within a tree crown is composed by branches and leaves/needles. The densities of branches and leaves (needles) are assumed to be uniform within the crown. Other cells include gap, trunk, and ground cells in the model.

B. Backscattering of the 3-D Forest Stand

Instead of the Muller matrix of a cell used in the Sun and Ranson model, the scattering matrix of a cubic cell is calculated in the new model to express both the terms of phase and backscattering coefficients. The coherent interactions between branches and leaves/needles within the crown cell are ignored. The phase of a signal received by the SAR antenna from a cubic cell is determined by the distance traveled by the radar wave. The distance traveled by the radar wave or time delay determines which image pixel this signature should be in. The signals located within the same SAR image pixel are coherently added to form the value of the pixel. The more detailed descriptions are as follows.

A forest stand is illuminated by a plane wave \vec{E}^i in the direction of \vec{k}_i . After the interaction with the forest stand, the electric wave \vec{E}^s is scattered into the direction of \vec{k}_s . The zenith and azimuth angles of the incidence wave are θ_i and ϕ_i while that of the scattered wave are θ_s and ϕ_s . If there are M forest cells (i.e., the cubic cells located within the crown or trunk) and N ground surface cells projected within a SAR image pixel, the total scattered field within the SAR pixel can be written as

$$\vec{E}_s = \left(\sum_{n=1}^M \vec{E}_n^s \right) + \left(\sum_{n=1}^N \vec{E}_{gn}^s \right). \quad (1)$$

\vec{E}_n^s is the scattered field from the n_{th} forest cell while \vec{E}_{gn}^s is the direct backscattering from a ground cell within the

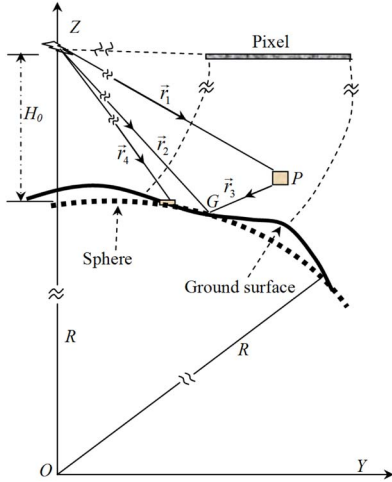


Fig. 2. Scattering components and their paths used in the model.

pixel. Only the first-order scattering is considered to keep the calculation tractable. The scattering field \vec{E}_{tn}^s consist of four scattering components: (a) the direct backscattering from the cell \vec{E}_{tn}^s ; (b) the scattering from ground toward the cell and then further scattered by the cell to radar \vec{E}_{tn}^{gs} ; (c) the scattering through the same path as (b) but in the opposite direction \vec{E}_{tn}^{sg} ; and (d) the multiple scattering between the cell and ground \vec{E}_{tn}^{sgs} , i.e., radar \rightarrow ground \rightarrow cell \rightarrow ground \rightarrow radar.

In the backscattering case, these components can be expressed as

$$\vec{E}_{tn}^s = e^{ik_0 l_1} \bar{T}_n^i \bar{S}_n^s(\theta_i, \phi_i; \pi - \theta_i, \phi_i - \pi) \bar{T}_n^t \vec{E}^i \quad (2)$$

$$\vec{E}_{tn}^{gs} = e^{ik_0 l_2} \bar{T}_n^i \bar{S}_n^s(\pi - \theta_i, \phi_i; \pi - \theta_i, \phi_i - \pi) \bar{T}_n^r \bar{R} \bar{T}_n^t \vec{E}^i \quad (3)$$

$$\vec{E}_{tn}^{sg} = e^{ik_0 l_3} \bar{T}_n^t \bar{R} \bar{T}_n^r \bar{S}_n^s(\theta_i, \phi_i; \theta_i, \phi_i - \pi) \bar{T}_n^i \vec{E}^i \quad (4)$$

$$\vec{E}_{tn}^{sgs} = e^{ik_0 l_4} \bar{T}_n^t \bar{R} \bar{T}_n^r \bar{S}_n^s(\pi - \theta_i, \phi_i; \theta_i, \phi_i - \pi) \bar{T}_n^r \bar{R} \bar{T}_n^t \vec{E}^i \quad (5)$$

where l_1 , l_2 , l_3 , and l_4 are the path length of radar waves in these scattering components. The path length of each scattering component is shown in Fig. 2. The expression of l_1 , l_2 , l_3 , and l_4 are $2|\vec{r}_1|$, $|\vec{r}_2| + |\vec{r}_3| + |\vec{r}_1|$, $|\vec{r}_1| + |\vec{r}_3| + |\vec{r}_2|$, and $2(|\vec{r}_2| + |\vec{r}_3|)$, respectively. k_0 is the wavenumber in free space. The changes of wavenumber within the forest canopy were ignored. \vec{r}_1 , \vec{r}_2 , and \vec{r}_3 denote the range vector from the antenna to the canopy cell, the vector from the antenna to the ground surface cell corresponding with the canopy cell, and the vector from the canopy cell to the ground cell, respectively.

\bar{S}_n^s is the scattering matrix of the n_{th} cell in the specified direction. The crown cell consists of the branches and leaves with given size and orientation distributions. The scattering matrix can be described as

$$\bar{S}_n^s = n_b \sum_{i=1}^m p_{\alpha_i} p_{\beta_i} p_l p_r \bar{S}_b(\alpha_i, \beta_i, l_i, r_i, \vec{k}_i, \vec{k}_s) + n_l \sum_{j=1}^n p_{\alpha_j} p_{\beta_j} \bar{S}_l(\alpha_j, \beta_j, \vec{k}_j, \vec{k}_s) \quad (6)$$

where \bar{S}_b is the scattering matrix of a branch with orientation angles α_i and β_i , length l_i , and radius r_i and p_{α_i} , p_{β_i} , p_l , and p_r are the corresponding probability density functions. \bar{S}_l is the scattering matrix of leaves or needles with orientations α_j and

β_j and p_{α_j} and p_{β_j} are the corresponding probability density functions. n_b and n_l are the numbers of branches and leaves (or needles) per cubic meter. The model used to calculate \bar{S}_b and \bar{S}_l is determined by the relative size of the scatterer and radar wavelength. For small leaves of deciduous trees or coniferous needles with a length less than 10% of the wavelength, the Rayleigh approximation is applied [11]. For large disk-shaped leaves, each leaf is modeled as a resistive sheet, and the physical optics approximation is adopted [12]. Trunks and large branches are modeled as finite-length dielectric cylinders. The field inside the finite cylinder is calculated using the infinite-length approximation [11]. For dielectric thin disks or cylinders whose sizes are smaller or comparable to the wavelength, a generalized Rayleigh–Gans model [13] has been implemented. This approximation requires that at least one dimension of an object is small with respect to the wavelength. Its inner field is approximated as a homogeneous field along this dimension, while phase differences in the other two dimensions must be accounted for [14].

A specular reflection matrix \bar{R} is calculated using the surface Fresnel reflection coefficient matrix, multiplied by a factor of $\exp[-2(k_0 \sigma \cos \theta)^2]$ to take into account the surface roughness effect [15], where σ is the root-mean-square height of the surface.

\bar{T}_n^i and \bar{T}_n^r denote the transmissivity matrices in the incidence and reflection directions, respectively. \bar{T}_n^t is the transmissivity matrix from the canopy cell to ground surface. According to Lin and Sarabandi [16], the Foldy–Lax approximation is used in the calculation of transmissivity matrices. The elements of the transmissivity matrix of a canopy cell can be expressed as

$$\bar{T}_{\hat{q}\hat{p}}^u(L) = e^{iM_{\hat{q}\hat{p}}L} \quad (7)$$

where \hat{q} , $\hat{p} = \hat{v}$, and \hat{h} are the incidence and scattered polarization of the electric wave. L is the traveling length of the electric wave in a canopy cell. The expression $M_{\hat{q}\hat{p}}$ can be denoted by

$$M_{\hat{q}\hat{p}} = \frac{2\pi}{k_0} S_{n,\hat{q}\hat{p}}^f \quad (8)$$

where $S_{n,\hat{q}\hat{p}}^f$ is the forward scattering matrix. If m canopy cells are passed when the electric wave travels from the antenna to the n_{th} cell, the transmissivity matrix can be calculated as

$$T_{n,\hat{q}\hat{p}}^i = [T_{\hat{q}\hat{p}}^u(L)]^m = T_{\hat{q}\hat{p}}^u(mL). \quad (9)$$

In this model, the branches and leaves (or needles) are uniformly distributed within canopy cells, and therefore, the transmissivity matrix can also be calculated as follows.

1) For copolarization ($\hat{q} = \hat{p}$)

$$T_{n,\hat{q}\hat{p}}^i = T_{\hat{q}\hat{p}}^u(mL) = e^{iM_{\hat{q}\hat{p}}mL}. \quad (10)$$

2) For cross-polarization ($\hat{q} \neq \hat{p}$)

$$T_{n,\hat{q}\hat{p}}^i = \underbrace{e^{iM_{\hat{q}\hat{q}}L} e^{iM_{\hat{p}\hat{p}}L} \dots}_{m} = e^{i(M_{\hat{q}\hat{q}} + M_{\hat{p}\hat{p}}) \frac{mL}{2}}. \quad (11)$$

\vec{E}_{gn}^s in (1) denotes the direct backscattering of ground surface. For the direct backscattering of the ground surface in a

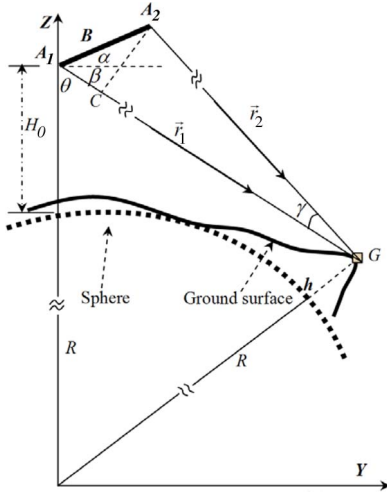


Fig. 3. Geometry relationships for InSAR configuration.

different location, the radar signal will undergo different canopy attenuation. \vec{E}_{gn}^s can be expressed as

$$\vec{E}_{gn}^s = e^{ik_0 l_5} \bar{T}_n^i \bar{S}_n^g(\theta_i, \phi_i; \pi - \theta_i, \phi_i - \pi) \bar{T}_n^i \vec{E}^i \quad (12)$$

where \bar{S}_n^g is the ground backscattering matrix of the n th ground surface cell. Considering the randomness of the phase of ground backscattering, \bar{S}_n^g is specified by the backscattering amplitude calculated by the integral equation model [17] and a random phase. $l_5 = 2|\vec{r}_4|$, where \vec{r}_4 is the range vector from the antenna to the ground surface cell.

The first item in (1) included all the scattering components related to the n th cell. However, some of the scattering components may be at the outside of the SAR image pixel when the n th cell located at the edge of the forest scene. Equation (1) can also be written as

$$\vec{E}_s = \sum_{n=1}^{M'} \left[\left(d_s \vec{E}_{tn}^s + d_{gs} \left(\vec{E}_{tn}^{gs} + \vec{E}_{tn}^{sg} \right) + d_{gsg} \vec{E}_{tn}^{gsg} \right)_{crown} + \left(d'_s \vec{E}_{tn}^s + d'_{gs} \left(\vec{E}_{tn}^{gs} + \vec{E}_{tn}^{sg} \right) \right)_{trunk} \right] + \sum_{n=1}^N d_g \vec{E}_{gn}^s \quad (13)$$

where $d_s, d_{gs}, d_{gsg}, d_g, d'_s,$ and $d'_{gs} = 0$ or 1 depend on whether the corresponding scattering components are located within the SAR image pixel.

C. Estimation of HSPC

The interferometric SAR images can be simulated using the SCSR model by placing the SAR antenna at two different positions. The position of the SPC can be retrieved from the simulated InSAR data. Fig. 3 shows the basic InSAR configuration with two antennae A_1 and A_2 . The altitude of antenna A_1 is H_0 . The baseline length is B . α is the baseline angle with respect to the horizontal direction. θ is the look incidence angle with β as its complementary angle. For simplicity, the Earth surface is modeled as a sphere with radius R . G is a point above the sphere. \vec{r}_1 and \vec{r}_2 are the range vectors from the two antennae to point G .

According to the cosine theorem, the elevation of point G can be expressed as

$$h = \sqrt{(R + H_0)^2 + |\vec{r}_1|^2 - 2(R + H_0)|\vec{r}_1| \cos \theta} - R. \quad (14)$$

In (14), $R, H_0,$ and $|\vec{r}_1|$ are known, and only the look angle θ needs to be determined. As shown in Fig. 3, A_2C is the perpendicular components of the baseline. From the geometry relationship, we can get

$$\begin{cases} A_1C + CG = |\vec{r}_1| \\ A_2C = B \sin(\alpha + \beta) = A_2G \sin \gamma \\ |\vec{r}_1| - |\vec{r}_2| = \lambda \frac{\Delta \phi}{2\pi} \end{cases} \Rightarrow \begin{cases} B \cos(\alpha + \beta) + |\vec{r}_2| \cos \gamma = |\vec{r}_1| \\ B \sin(\alpha + \beta) = |\vec{r}_2| \sin \gamma \\ |\vec{r}_1| - |\vec{r}_2| = \lambda \frac{\Delta \phi}{2\pi}. \end{cases} \quad (15)$$

In (15), λ is the radar wavelength. $\Delta \phi$ is the phase difference from simulated InSAR data. There are three unknown variables ($\beta, \gamma,$ and $|\vec{r}_2|$) and three independent equations. Therefore, β can be determined, and θ can further be determined

$$\theta = \frac{\pi}{2} - \left(\cos^{-1} \left(\frac{B^2 + 2|\vec{r}_1| \frac{\Delta \phi}{2\pi} \lambda - \left(\frac{\Delta \phi}{2\pi} \lambda \right)^2}{2B|\vec{r}_1|} \right) - \alpha \right). \quad (16)$$

The height of scattering phase center (HSPC) is the difference between the elevation of SPC and that of the ground surface.

III. MODEL VERIFICATION

Model verification is the prerequisite of the model-based analysis of the influences of forest structure on the SPC. The full validation of a coherent radar backscatter model would require high-quality PolInSAR data as well as extensive field measurements. Because of the lack of high-quality L-band PolInSAR data, the performance of the behavior of the SCSR model was verified in two ways. First, layered forest scenes with homogeneous horizontal structure were used to simulate the dependence of HSPC on the vertical height and structure of the canopy at L-band. Then, the simulated HSPC at C-band was compared with those derived from SRTM and the ground surface elevation from National Elevation data provided by the United States Geological Survey.

A. Simulation of Layered Forest Scenes

The model was first examined under the simplest forest scene, i.e., the single-layer forest scene. The single-layer forest scene consists of a layer of cubic cells at a given height as crown cells. Move up the layer gradually at a step of the layer's thickness as shown in Fig. 4(a) to examine the behavior of the HSPC. The model was then examined under a more complicated forest scene than a single-layer one, i.e., a multiple-layer forest scene. Add crown layers one by one over the top of the previous layers as shown in Fig. 4(b) to observe the behavior of the HSPC. The incidence angle was assumed as 35° while the width of the cubic cell was 0.5 m. For the calculation simplicity of the transmission path length, the cell thickness should be 0.714 m (i.e., $0.5 \text{ m}/\tan 35^\circ$) to make the electric wave passing

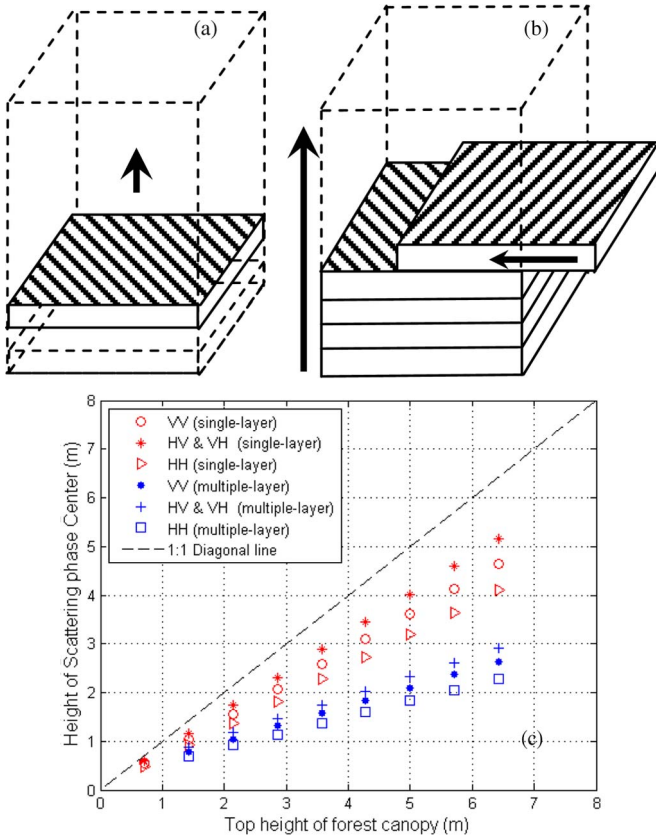


Fig. 4. Examination of model by layered forest scenes at L-band. (a) Single-layer forest scene: One canopy layer moving upward. (b) Multiple-layer forest scene: Adding canopy layers one by one. (c) Simulated HSPC of (a) and (b).

through the diagonal of a cell. A canopy layer is moved upward from 0.714 m (the top height of the first layer) to 6.426 m (the top height of the ninth layer) in Fig. 4(a). The canopy height increased at a step of the thickness of the layer (i.e., cell thickness). The forest canopy thickness of the multiple-layer forest scene gradually increased from 1.428 m (two layers) to 6.426 m (nine layers) in Fig. 4(b). The wavelength was L-band (i.e., 0.235 m). The baseline length was set to be 400 m, and the baseline tilt angle was -20° .

Simulated results were shown in Fig. 4(c). The horizontal axis was the top height of a forest scene while the vertical axis was the HSPC from modeling. For the layered forest scene, the model consisted of five scattering components, i.e., \vec{E}_{tn}^s , \vec{E}_{tn}^{gs} , \vec{E}_{tn}^{sg} , \vec{E}_{tn}^{gsg} , and \vec{E}_{gn}^s . Their corresponding HSPCs were expressed as h_{tn}^s , h_{tn}^{gs} , h_{tn}^{sg} , h_{tn}^{gsg} , and h_{gn}^s . The results showed that the HSPC increased linearly with the increases of the layer height or thickness. These results were expected. h_{tn}^s should be equal to the center height of the top layer. h_{tn}^{gs} , h_{tn}^{sg} , and h_{gn}^s should be zero while h_{tn}^{gsg} should be $-h_{tn}^s$. However, the amplitudes of the last four components should be much smaller than \vec{E}_{tn}^s because \vec{E}_{tn}^{gs} , \vec{E}_{tn}^{sg} , and \vec{E}_{tn}^{gsg} were reflected by the cubic cell as well as by the ground surface while \vec{E}_{gn}^s was attenuated by the crown layer. Therefore, \vec{E}_{tn}^s was the dominant factor. The HSPC should increase along with the layer height or thickness. The HSPC should also be lower than the top height of the forest canopy due to the contribution of double bounces (i.e., \vec{E}_{tn}^{gs} , \vec{E}_{tn}^{sg} , and \vec{E}_{tn}^{gsg}) and ground backscattering (i.e., \vec{E}_{gn}^s). Fig. 4(c) showed that the HSPC of the single-

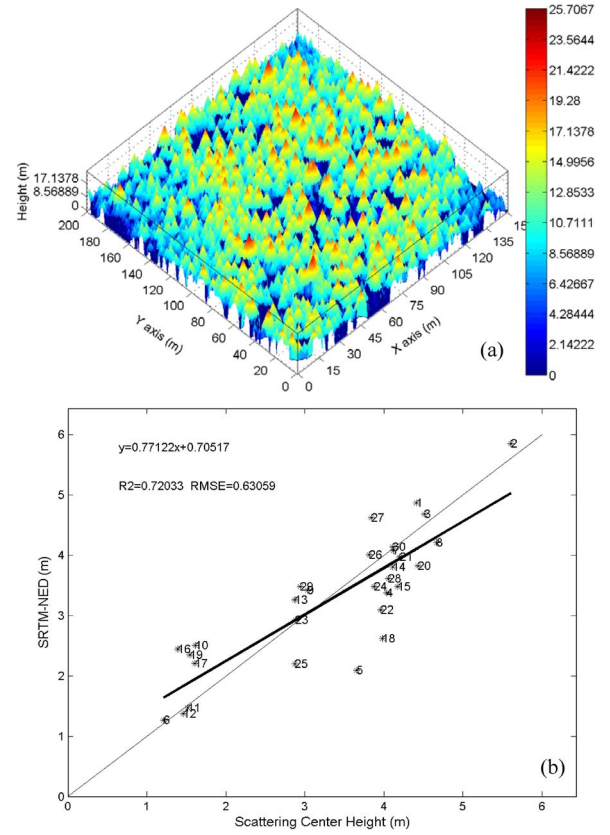


Fig. 5. Validation of the SCSR model using field measurement at C-band. (a) Forest canopy top surface of test site. (b) Simulated and observed HSPCs. The horizontal axis is the simulated HSPC while the vertical axis is the HSPC derived from SRTM.

layer forest scene was higher than that of the multiple-layer one with the same top height because the contributions from the underlying layers and the double bounces pulled down the HSPC of the multiple-layer forest scene. These reasonable phenomena demonstrated the soundness of the model under the layered forest scene.

B. Simulation at C-Band and Comparison With SRTM Data

The SCSR model was further validated by the C-band InSAR data (SRTM) at a test site in Maine. The 3 ha (200 m \times 150 m) field plot is located at the International Paper's Northern Experiments Forest located near Howland, Maine, USA ($45^\circ 12' N$, $65^\circ 45' W$). The Cartesian stem location, DBH, tree species, and relative canopy position have been recorded for each stem with DBH > 3 cm. It is a mixed conifer and northern hardwood stand composed of over 90% conifers (mostly spruce and hemlock) [10]. The 3-D forest scene was shown as Fig. 5(a). Heights were estimated from the relationships between DBH and height developed from field measurements. Diameter and height distributions were detailed in [18]. The detailed measurements of the branch size and orientation of hemlock trees, dielectric constants of trees, roughness and dielectric constants of ground surface were described in [19].

The plot was divided into 30 subplots of 30 m \times 30 m which was about the same size as a pixel of SRTM data (1 arc-second). The stand data of the subplots (i.e., the tree size, positions, species, and dielectric constants) were used to

build the 3-D forest scene. Then, the SCSR model was used to simulate the InSAR data and to retrieve the HSPC. The system parameters used in the simulation were wavelength = 5.6 cm, incidence angle = 35°, baseline length = 62 m, and baseline angle = 60° [20]. The comparison of the HSPC derived from SRTM and that retrieved from simulated InSAR data was shown in Fig. 5(b). It was clear that the simulated results were consistent with observations.

IV. MODEL SIMULATION ANALYSIS

A. Scheme for Simulation Analysis

Forest density and forest height are important factors determining the forest carbon storage. These two factors are always coupled in heterogeneous forest. A set of homogeneous forest stands was first simulated to investigate the sensitivity of the position of the SPC to forest density and forest height separately. To form a series of stands with different heights, 19 trees of the same size were scattered within a 30 m × 30 m plot. The heights of these trees increased from 5 to 40 m with an interval of 1 m. The crown depth was 0.6 × tree height while the crown width was 0.5 × tree height. For the simulation of forest stands with different densities, trees were put into a 30 m × 30 m plot one by one from 1 to 70. Tree height was 28 m with crown depth of 16 m and crown width of 14 m. In the process of building 3-D forest scenes, if the crown of an added tree overlapped with the crowns of existing trees, the new crown was ignored. Therefore, cells of overlapping crowns only have the property of the crown of the first tree.

Homogeneous forest enabled us to analyze the effect of forest height and density on the position of the SPC separately. However, it had to be admitted that some cases of homogeneous forests were rare or even did not exist in reality. Therefore, a set of heterogeneous forests generated from a forest growth model was also simulated using the SCSR model. The forest growth model (ZELIG) had been parameterized in research sites by Ranson *et al.* [21]. The heterogeneous forests were generated at five-year intervals up to 500 years. Because the ZELIG model possesses underlying stochasticity in tree regeneration, mortality, and weather routines, 15 duplicative runs were conducted to generate a range of stand responses. In total, 1500 forest stands were simulated. The 3-D forest scenes built from these 1500 forest stands were fed into the SCSR model to simulate their corresponding HSPCs. The interferometric system parameters used here were the same as those used in Section III-A. The structures of these heterogeneous forests were defined by four height indexes: a) Maximum height—the height of the tallest tree within a forest stand; b) Mean height—the average height of all trees within a forest stand; c) Lorey's height (i.e., basal area weighted mean height)—it was calculated by multiplying each tree height by its basal area and then dividing the sum of this calculation by the total stand basal area; and d) Crown size-weighted height (CWH)—the average height of each tree weighted by its crown size as proposed by Pang *et al.* [22].

The HSPC was the distance from ground surface to the SPC. It was the difference between the elevation of the SPC and that of ground surface. However, it was difficult to get ground elevation over forest areas even by lidar data, particularly over dense tropical rain forest. It was easy to obtain the elevation of the forest canopy top by lidar or high-resolution stereo im-

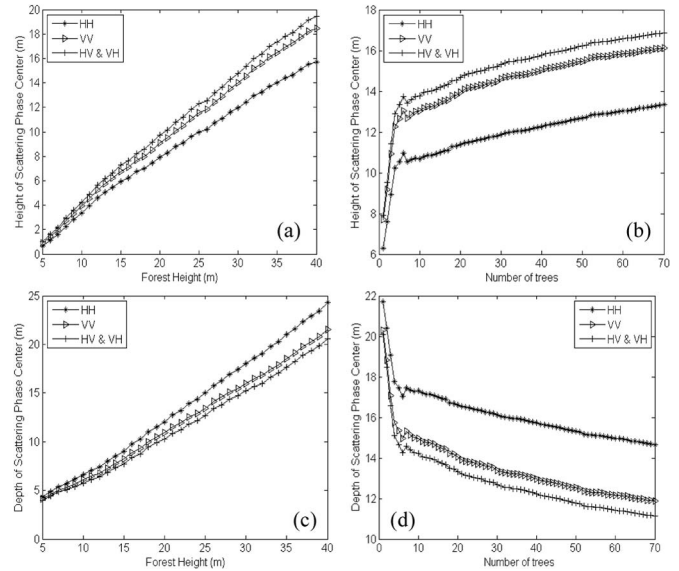


Fig. 6. Effects of forest structures of homogeneous forest on the SPC at L-band. (a) Effect of forest height on the HSPC. (b) Effect of forest density on the HSPC. (c) Effect of forest height on the DSPC. (d) Effect of forest density on the DSPC.

ages. Herein, a new variable “depth of scattering phase center” (DSPC) was defined to describe the position of the SPC. DSPC was defined as the distance from the forest canopy top to the SPC. The CWH serves as the height of the forest canopy top in this study because it can be directly derived from lidar data. The relationships between the HSPC, DSPC, and forest height indices were explored.

B. Results

Fig. 6 showed the effects of forest structures on the HSPC in homogeneous forests. Fig. 6(a) and (c) showed that the HSPC and DSPC increased nearly linearly with the increase of forest height. The separation between cross-polarization and copolarization also became larger for tall stands. Fig. 6(b) and (d) showed that the HSPC and DSPC were sensitive to forest stem density when the forest was sparse. The sensitivity of the HSPC and DSPC to forest density significantly decreased when there were more than seven trees in a forest stand.

Fig. 7(a) showed the changes of the HSPC and DSPC at L-band (HH polarization) of one duplicate along with the forest age. It was shown that the HSPC increased rapidly as the young forest grows. When forests mature (greater than 200 years old), the HSPC fluctuated around a certain value (about 8 m in this case). It was clear that the effect of forest density on the HSPC was very weak. The decrease of forest density from 50 to 190 years and the increase from 190 to 210 years were not reflected on the HSPC. This was consistent with the result of homogeneous forest. For forest stands younger than 20 years old, their HSPC were lower than DSPC. Both HSPC and DSPC increased as the forest is growing, and the HSPC was higher than the DSPC until the forest became mature (greater than 200 years old). Then, the HSPC and DSPC fluctuated around each other and a certain value. Comparing the maximum height and the CWH, it was clear that the CWH was more stable in the description of the state of the forest stand than the maximum height. The effect of the death of the tallest tree on CWH,

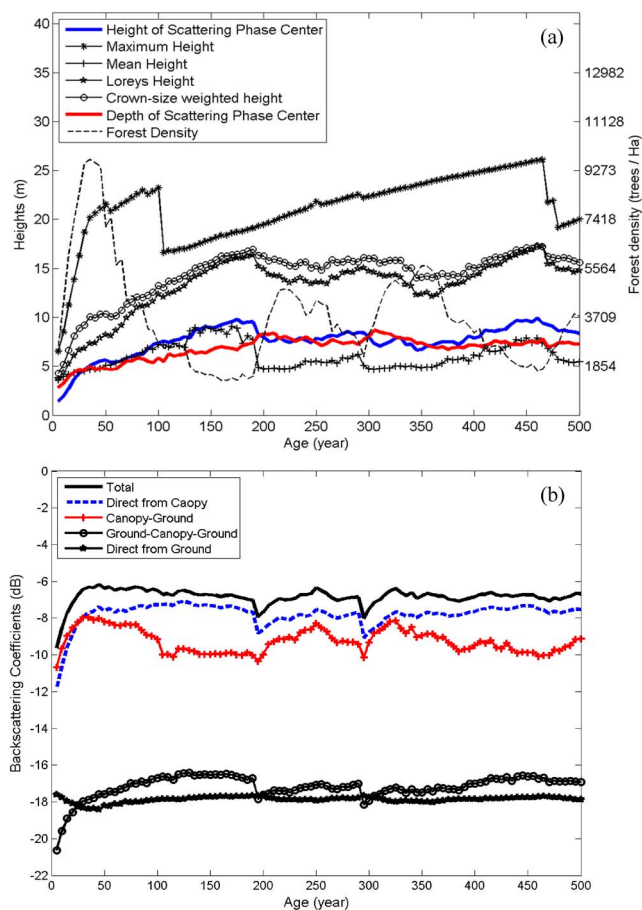


Fig. 7. Effects of forest structures of heterogeneous forest on (a) HSPC and on (b) the backscattering coefficients at L-band (HH).

such as for the forest stands aged around 90 years and around 445 years, was much smaller than that on the maximum height. The overall trend of CWH was consistent with Lorey’s height, although there was a small difference in absolute value over some ages.

Fig. 7(b) shows the backscattering coefficients from different scattering components which were also the indications of the contributions of different components to the HSPC. For a young forest, the canopy-ground double bounce was the dominant component. The contribution of the direct backscattering from the forest canopy increased along with the forest age and became dominant after 30 years. Forest stands younger than 30 years old could be deemed to be homogeneous forest because they exhibited the same behavior as homogeneous forest in Fig. 6 that the HSPC and DSPC increased steadily along with the increase of forest height and forest density. Although the direct backscattering from the forest canopy was the dominant term after 30 years, the contributions from other components were still important, particularly the canopy-ground double bounce. The canopy-ground double bounce pulled down the HSPC because its SPC was near ground surface. The decrease of the contribution from the canopy-ground double bounce caused the increase of the HSPC from 30 to 200 years.

Fig. 8 shows the array of scatterplots of the forest height indices against the position of the SPC expressed as the HSPC or the DSPC of all 15 duplicates. The four columns from left to right were for the maximum height, CWH, Lorey’s height, and mean height, respectively. Each row was for the results

of one polarization. The first three rows were for the HSPC (HH, HV, and VV up to down) while the last three were for the DSPC. Fig. 8(c), (g), and (k) showed that the HSPC was highly correlated with Lorey’s height with R^2 of 0.945, 0.978, and 0.945 at HH, HV, and VV polarizations, respectively. Fig. 8(b), (f), and (j) showed that the HSPC was also correlated with the CWH with R^2 of 0.899, 0.940, and 0.918, respectively. As shown in Fig. 8(a), (e), and (i), the maximum height was correlated with the HSPC when forests were young. Fig. 8(d), (h), and (l) also showed the correlation between the HSPC and mean height of the young forest. Fig. 8(n) and (v) showed that the copolarized DSPC was highly correlated with CWH with R^2 of 0.878 and 0.905, respectively. The copolarized DSPC was also correlated with Lorey’s height with R^2 of 0.830 and 0.905 as shown in Fig. 8(o) and (w).

V. DISCUSSIONS

In the model verification using SRTM data, the predictions derived from the model are not perfect. The errors may be caused by several factors. First, the dynamic range of the incidence angle of C-band SAR images of SRTM was from 30° to 60° . The exact incidence angle and polarization is unknown at the plot site. It is also difficult to exactly match the subplot with SRTM pixels, although they have the same size because of the mismatching between the radar-looking direction and the orientation of subplots.

In this paper, in addition to the “height” of the scattering phase center (HSPC), the “depth” of the scattering phase center (DSPC) is proposed to describe the position of SPC. It has to be underlined that the DSPC is not the penetration degree but the penetration depth, i.e., the product of the penetration degree and forest height. Theoretically, forest biomass should be negatively correlated with penetration degree but positively correlated with DSPC. As shown in Fig. 6(c), the penetration degree is 80% under a 5-m-tall forest with penetration depth = 4 m while the penetration degree at HH is 60% under a 40-m-tall forest with the penetration depth = 24 m. An exception is that the increase of forest biomass is not because of the forest growth but due to the increase of forest density as shown in Fig. 6(d). This situation generally does not appear in heterogeneous forest as shown in Fig. 8.

The DSPC is defined in this study by the distance from the SPC to the reference point assigned by the CWH. The CWH is not the only way to define the DSPC. The critical issue in the definition of the DSPC is that the height index representing the top height of the forest canopy should stably describe the state of the forest stand. Otherwise, the correlation between the DSPC and forest biomass will be overwhelmed if the height index can be easily affected by the changes of a few trees.

Fig. 8 showed that the DSPC correlated with CWH and Lorey’s height only at copolarization. The loss of correlation between the DSPC and CWH or Lorey’s height at cross-polarization may be attributed to the smaller penetration depth at cross-polarization than that at copolarization. It can be seen from Fig. 8(n) and (r) that the gains of the regression equation between the DSPC and CWH are 0.474 and 0.138 at HH and HV, respectively. That is to say, the average penetration degree is 47.4% at HH while it is only 13.8% at HV. The sensitivity of penetration depth to CWH at HV may be masked by the disturbance of forest structures on DSPC at HV.

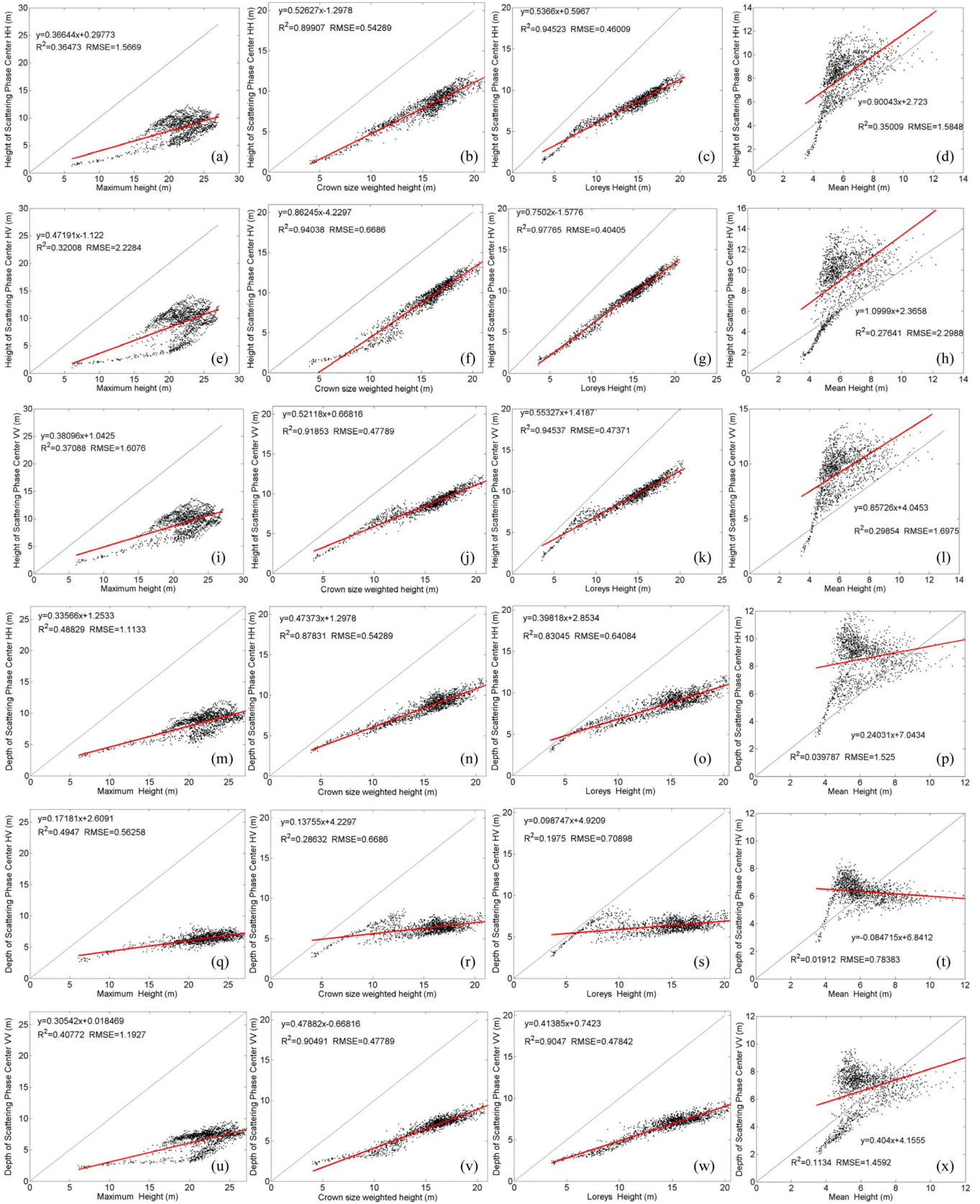


Fig. 8. Correlations between the position of the SPC at L-band and forest height indices. The horizontal axis is the forest height index while the vertical axis is the position of the SPC expressed as the HSPC or the DSPC and derived from different polarizations.

As pointed out in a previous section, the forest younger than 30 years old could be deemed to be homogeneous forest because its height and density increased steadily along with

forest age. The structures of forest older than 30 years were complicated by the tree mortality and regeneration. Fig. 7(a) showed that the maximum height, CWH, Lorey's height, and

mean height of homogeneous forest were lower than 20, 10, 8, and 5 m, respectively. Fig. 8 showed that the behavior of homogeneous forest on InSAR data was quite different from that of heterogeneous forest. Both the HSPC and DSPC of all polarizations had excellent correlations with all the four height indices of homogeneous forest, but that was not the case for heterogeneous forest. Therefore, it was relatively easy to develop algorithms of forest biomass for homogeneous forest. Special care was needed when these retrieval algorithms were applied on heterogeneous forest.

Saatchi *et al.* mapped the forest carbon stocks in tropical regions across three continents [23]. One of the critical steps of their study was to build the relationship between lidar-derived Lorey's height and above ground biomass. The correlation between the HSPC and Lorey's height provided a theoretical base for the extrapolation of lidar-estimated biomass to the entire region through the combination of lidar and InSAR data. Nevertheless, the disturbance from the temporal decorrelation of InSAR should be first analyzed before the method becomes practical.

The derivation of the HSPC from InSAR needs the ground surface elevation under the forest. As mentioned in the previous section, the acquisition of ground surface elevation is not easy at dense forest. The correlation between the DSPC and Lorey's height at copolarization provides a potential way to estimate forest biomass without ground surface elevation. The derivation of the DSPC from InSAR is easy relative to the HSPC because it only needs the top height of the forest canopy. The information of the forest canopy top may be acquired from high-resolution stereo images, lidar data, or short-wavelength InSAR data.

VI. CONCLUSION

The estimation of forest biomass from SAR data is always limited by the signal saturation problems due to the lack of forest structure information. The crucial issue is to parameterize the forest structure and to link the parameter to remote-sensing observations. The InSAR data provide information on forest vertical structures, particularly at long wavelength. However, the mixture of contributions from upper and lower parts of the forest complicates the interpretation of long-wavelength InSAR data. The understanding of the influence of forest structure on the position of the SPC is critical for the interpretation and exploits of long-wavelength InSAR data. In this paper, a new semicoherent model (SCSR) was developed based on the Sun and Ranson [10] model. The influence of forest structures on the position of the SPC was simulated by the SCSR model at L-band under both homogeneous and heterogeneous forest conditions. Aside from the HSPC, the DSPC was also proposed to express the InSAR observations. The simulations showed that both the HSPC and DSPC at all polarizations were positively correlated with forest height under homogeneous forest. The HSPC of heterogeneous forest was highly correlated with Lorey's height and CWH at all polarizations while the DSPC of heterogeneous forest positively correlated with Lorey's height and CWH at copolarization. The retrieval algorithm of forest biomass or height developed on homogeneous forest may not be applicable to heterogeneous forest. The DSPC was a measurable variable which may be obtained through the combination of InSAR data and lidar or high-resolution photogrammetry data. A potential way for the estimation of forest biomass is the data synergy of InSAR data with lidar or high-resolution

stereo images. The effect of temporal decorrelation in repeat-pass InSAR data on these findings will be further explored using PALSAR InSAR data in our future research.

REFERENCES

- [1] M. Lefsky, D. Harding, M. Keller, W. Cohen, C. Carabajal, F. Espirito-Santo, M. Hunter, and R. de Oliveira, Jr., "Estimates of forest canopy height and aboveground biomass using ICESat," *Geophys. Res. Lett.*, vol. 32, no. 22, pp. 1–4, Nov. 2005.
- [2] T. Neeff, L. V. Dutra, J. R. dos Santos, C. D. Freitas, and L. S. Araujo, "Tropical forest measurement by interferometric height modeling and P-band radar backscatter," *Forest Sci.*, vol. 51, no. 6, pp. 585–594, Dec. 2005.
- [3] H. Balzter, A. Luckman, L. Skinner, C. Rowland, and T. Dawson, "Observations of forest stand top height and mean height from interferometric SAR and LiDAR over a conifer plantation at Thetford Forest, UK," *Int. J. Remote Sens.*, vol. 28, no. 6, pp. 1173–1197, Mar. 2007.
- [4] J. Praks, F. Kugler, K. P. Papathanassiou, I. Hajnsek, and M. Hallikainen, "Height estimation of boreal forest: Interferometric model-based inversion at L- and X-band versus HUTSATC profiling scatterometer," *IEEE Geosci. Remote Sens. Lett.*, vol. 4, no. 3, pp. 466–470, Jul. 2007.
- [5] L. Thirion, E. Colin, and C. Dahon, "Capabilities of a forest coherent scattering model applied to radiometry, interferometry, and polarimetry at P-and L-band," *IEEE Trans. Geosci. Remote Sens.*, vol. 44, no. 4, pp. 849–862, Apr. 2006.
- [6] L. Thirion-Lefevre and E. Colin-Koeniguer, "Investigating attenuation, scattering phase center, and total height using simulated interferometric SAR images of forested areas," *IEEE Trans. Geosci. Remote Sens.*, vol. 45, no. 10, pp. 3172–3179, Oct. 2007.
- [7] D. W. Liu, G. Q. Sun, Z. F. Guo, K. J. Ranson, and Y. Du, "Three-dimensional coherent radar backscatter model and simulations of scattering phase center of forest canopies," *IEEE Trans. Geosci. Remote Sens.*, vol. 48, no. 1, pp. 349–357, Jan. 2010.
- [8] D. W. Liu, Y. Du, G. Q. Sun, W. Z. Yan, and B.-I. Wu, "Analysis of InSAR sensitivity to forest structure based on radar scattering model," *Progr. Electromagn. Res.*, vol. 84, pp. 149–171, 2008.
- [9] F. Garestier and T. Le Toan, "Forest modeling for height inversion using single-baseline InSAR/Pol-InSAR data," *IEEE Trans. Geosci. Remote Sens.*, vol. 48, no. 3, pp. 1528–1539, Mar. 2010.
- [10] G. Sun and K. J. Ranson, "A three-dimensional radar backscatter model of forest canopies," *IEEE Trans. Geosci. Remote Sens.*, vol. 33, no. 2, pp. 372–382, Mar. 1995.
- [11] L. Tsang, J. A. Kong, and R. T. Shin, *Theory of Microwave Remote Sensing*. New York, NY, USA: Wiley, 1985.
- [12] F. T. Ulaby, K. Sarabandi, K. McDonald, M. Whitt, and M. C. Dobson, "Michigan Microwave Canopy Scattering Model (MIMICS)," in *Proc. Int. Geosci. Remote Sens. Symp. Remote Sens., Moving Toward 21st Century*, 1988, p. 1009.
- [13] M. A. Karam, A. K. Fung, and Y. M. M. Antar, "Electromagnetic wave scattering from some vegetation samples," *IEEE Trans. Geosci. Remote Sens.*, vol. 26, no. 6, pp. 799–807, Nov. 1988.
- [14] J. Du, J. Shi, S. Tjuatja, and K. S. Chen, "A combined method to model microwave scattering from a forest medium," *IEEE Trans. Geosci. Remote Sens.*, vol. 44, no. 4, pp. 815–824, Apr. 2006.
- [15] A. Ishimaru, *Wave Propagation and Scattering in Random Media*. New York, NY, USA: Academic, 1978.
- [16] Y. C. Lin and K. Sarabandi, "A Monte Carlo coherent scattering model for forest canopies using fractal-generated trees," *IEEE Trans. Geosci. Remote Sens.*, vol. 37, no. 1, pp. 440–451, Jan. 1999.
- [17] A. K. Fung and K. S. Chen, *Microwave Scattering and Emission Models and their Applications*. Norwood, MA, USA: Artech House, 1994.
- [18] K. J. Ranson, J. A. Smith, and G. S. Center, "Airborne SAR experiment for forest ecosystems research Maine 1989 experiment," in *Proc. Int. Geosci. Remote Sens. Symp.*, 1990, pp. 861–864.
- [19] N. S. Chauhan, R. H. Lang, and K. J. Ranson, "Radar modeling of a boreal forest," *IEEE Trans. Geosci. Remote Sens.*, vol. 29, no. 4, pp. 627–638, Jul. 1991.
- [20] W. A. Imbriale, *Spaceborne Antennas for Planetary Exploration*. Hoboken, NJ, USA: Wiley, 2006, Online Library.
- [21] K. J. Ranson, G. Sun, R. G. Knox, E. R. Levine, J. F. Weishampel, and S. T. Fifer, "Northern forest ecosystem dynamics using coupled models and remote sensing," *Remote Sens. Environ.*, vol. 75, no. 2, pp. 291–302, Feb. 2001.
- [22] Y. Pang, M. Lefsky, M. Miller, K. Sherrill, and H. Andersen, "Automatic tree crown delineation using discrete return lidar and its application in ICESat vegetation product validation," *Can. J. Remote Sens.*, vol. 34, no. S2, pp. 471–484, Nov. 2008.

- [23] S. S. Saatchi, N. L. Harris, S. Brown, M. Lefsky, E. T. A. Mitchard, W. Salas, B. R. Zutta, W. Buermann, S. L. Lewis, S. Hagen, S. Petrova, L. White, M. Silman, and A. Morel, "Benchmark map of forest carbon stocks in tropical regions across three continents," *Proc. Nat. Acad. Sci. USA*, vol. 108, no. 24, pp. 9899–9904, Jun. 14, 2011.



Wenjian Ni (M'09) received the B.Eng. degree in surveying and mapping from the Shandong University of Technology, Zibo, China, in 2004 and the Ph.D. degree in cartography and geographic information system from the Graduate University of Chinese Academy of Sciences, Beijing, China, in 2009.

He worked as an Assistant Research Scientist in the Institute of Remote Sensing and Digital Earth, Chinese Academy of Sciences, Beijing, China, in 2009–2010. He is doing postdoctoral research in the Department of Geographical Sciences, University of Maryland, College Park, MD, USA, from July 2010. His research interests include measuring and modeling the radar backscattering of vegetated surface; description of a 3-D forest scene using terrestrial, airborne, or spaceborne laser scanner data; and algorithm exploration for the mapping of forest aboveground biomass at regional scale using multiple remote-sensing data.



Guoqing Sun (S'85–M'90–SM'99) received the B.S. degree in physics from the University of Science and Technology of China, Hefei, China, in 1970, the M.Sc. degree in remote sensing from Nanjing University, Nanjing, China, in 1981, and the Ph.D. degree in geography from the University of California, Santa Barbara, CA, USA, in 1990.

He is currently a Research Professor with the Department of Geographical Sciences and Earth Science System Interdisciplinary Center, University of Maryland, College Park, MD, USA, who is also affiliated with NASA's Goddard Space Flight Center, Greenbelt, MD, USA. He has been involved in research works on remote sensing and geographical-information-system applications since early 1980s and worked as a principal researcher and investigator in various NASA programs, Remote Sensing Science, Carbon Cycle, Terrestrial Ecosystem, and Carbon Monitoring System Programs. His current research includes radar backscatter and lidar waveform modeling of vegetated surface, remote-sensing data fusion for forest structure parameter retrieval, and land cover/land use change studies.

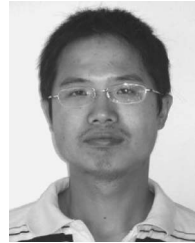
Dr. Sun is a former Chair of the Washington, DC–Northern Virginia Chapter of the IEEE Geoscience and Remote Sensing Society. He has been an Associate Editor of the *Canadian Journal of Remote Sensing* since 2007.



Kenneth Jon Ranson received the B.S. and M.S. degrees in earth resources from Colorado State University, Fort Collins, CO, USA, in 1972 and 1975, respectively, and the Ph.D. degree from Purdue University, West Lafayette, IN, USA, in 1983. His doctoral research involved the studies of the bidirectional reflectance characteristics of crops. His graduate studies involved research on the use of Skylab and Landsat multispectral scanner data for geologic and forest cover mapping.

He spent a year as a Postdoctoral Research Associate and another two years as a Professional Agronomist with the Laboratory for Applications of Remote Sensing, Purdue University. During this time, his research considered the reflectance behavior of vegetation canopies and the microwave backscatter characteristics of crops and trees. In 1986, he joined the Biospheric Sciences Laboratory, NASA Goddard Space Flight Center, Greenbelt, MD, USA, where he currently serves as the Laboratory Chief. He also continues his research on lidar and microwave interactions with forest canopies. Over the past several years, he has also conducted NASA-supported radar and lidar-based research of forests. In addition to his research activities, he was a Project Scientist for NASA's Earth Observing System Terra spacecraft and twice served as an acting NASA head quarters Program Manager.

Dr. Ranson is a member of the Geoscience and Remote Sensing Society and the American Geophysical Union.



Zhiyu Zhang received the B.S. degree in applied physics from the China University of Mining and Technology, Beijing, China, in 2005 and the Ph.D. degree in cartography and geographic information system from Beijing Normal University, Beijing, in 2011.

He is currently with the State Key Laboratory of Remote Sensing Science, jointly sponsored by the Institute of Remote Sensing and Digital Earth of Chinese Academy of Sciences and Beijing Normal University. His research interests include forest structure retrieval using lidar and radar data, interferometric-synthetic-aperture-radar data processing, and classification.



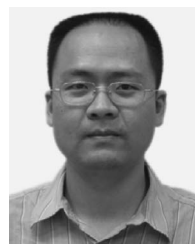
Yating He received the B.S. degree in biology science from Huaibei Normal University, Huaibei, China, in 2000, the M.Sc. degree in ecology from Wuhan Botanical Garden, Chinese Academy of Sciences, Wuhan, China, in 2007, and the Ph.D. degree from the Institute of Geographic Sciences and Natural Resources Research, Chinese Academy of Sciences, Beijing, China.

She is currently with the Institute of Agricultural Resources and Regional Planning, Chinese Academy of Agricultural Sciences, Beijing. Her research interests include the carbon/nitrogen cycle, effects of nitrogen fertilization on soil microbial ecology, impacts of land use/land cover on soil carbon storage, and ecophysiological characteristics of grassland ecosystem and cropland ecosystem.



Wenli Huang received the B.Sc. degree in computer cartography from Wuhan University, Wuhan, China, in 2006 and the M.Sc. degree in remote sensing and geographical information system from the Beijing Normal University, Beijing, China, in 2009. She is currently working toward the Ph.D. degree at the University of Maryland, College Park, MD, USA.

Her main research interest concerns the application of LiDAR and radar remote sensing for the retrieval of forest biophysical parameters.



Zhifeng Guo received the B.Eng. degree from the Wuhan Technical University of Surveying and Mapping, Wuhan, China, in 1999 and the M.S. degree in geographical information science and cartography and the Ph.D. degree in microwave remote sensing from the Institute of Remote Sensing Applications, Chinese Academy of Sciences, Beijing, China, in 2002 and 2005, respectively.

He is currently with Institute of Remote Sensing and Digital Earth of Chinese Academy of Sciences, Beijing. His research interests include 3-D realistic forest scene construction for synthetic aperture radar, lidar, and optical modeling and forest biophysical parameter inversion using multiple-sensor data.